2011 50th IEEE Conference on Decision and Control and
European Control Conference (CDC-ECC)
Orlando, FL, USA, December 12-15, 2011

A Switching Observer for Sensorless Control of an Electromagnetic Valve Actuator for Camless Internal Combustion Engines

Paolo Mercorelli

***Abstract*—In this paper, the design and operation of a special electromagnetic motor as a variable engine valve actuator are presented. Further, this paper presents feasible approximated velocity switching estimator based on measurements of current and input voltage to achieve sensorless control. This approach avoids a more complex structure for the observer and yields an particular control strategy with an acceptable performance. In general, this approach can represent a viable strategy to build reduced-order observer to estimate not only velocity but also position of a such as type of systems through the measurement of input current and input voltage. This control strategy is presented and discussed as well. Computer simulations of the sensorless control structure are presented in which results are visible in the closed-loop control.**

Key-words: Actuators, nonlinear systems, observability, observer, digital signal processors.

I. INTRODUCTION

In the last years, variable engine valve control has attracted a lot of attention because of its ability to reduce pumping losses (work required to draw air into the cylinder under part-load operation) and to increase torque performance over a wider rage than conventional spark-ignition engines. Variable valve timing also allows the control of internal exhaust gas recirculation, thereby improving fuel economy and reducing NOx emissions. Electromagnetic valve actuators have been reported in the past and recent works mark technical progress in this area, in particular, Refs. [1] and [2]. Theoretically, electromagnetic valve actuators offer the highest potential to improve fuel economy due to their control flexibility. In real applications, however, the electromechanical valve actuators developed so far mostly suffer from high power consumption and other control problems. Therefore, innovative concepts are required to reduce the losses while keeping the actuator dynamic. This contribution moves from the results already presented in [3] and shortly summarised in the first part of this paper. These theoretical and experimental results for the design of a novel permanent-magnet linear valve actuator are shown again, allowing short-stroke high-dynamic operations combined with low power losses. The original contribution of this work in presented in the second part of the paper where a sensorless control is analysed. To realise this goal, it is necessary to create an observer structure. In particular, a velocity observer is proposed which allow to avoid derivatives of the measured position which can generate undesired spikes and noise. Sensorless operations tend to perform poorly in low-speed environments, as nonlinear observer-based algorithms work only if the mover speed is high enough. In low-speed regions, an open loop control strategy must be considered. One of the first attempts to develop an observer for a permanent motor drive is described in Ref. [4]. In a more recent work [5], the authors proposed a nonlinear-state observer for the sensorless control of a permanent-magnet AC machine, based to a great extent on the work described in Refs. [6] and [7]. The approach presented in Refs. [6] and [7] consists of an observable linear system and a Lipschitz nonlinear part. The observer is basically a Luenberger observer, in which the gain is calculated through a Lyapunov approach. In Ref. [5], the authors used a change of variables to obtain a nonlinear system consisting of an observable linear part and a Lipschitz nonlinear part. In the work presented here, our system does not satisfy the condition in Ref. [7]; thus, a such as type of observer is not feasible. The paper is organised as follows. In Section II, a new actuator design is shown. Section III is devoted to the analysis of the model. Section IV shows the approximated velocity observer. In Section V, a control strategy is presented and discussed. Section VI presents computer simulations of the sensorless control structure, in which the positive results are visible in the closed-loop control. The conclusions and future work close the paper.

This work was supported by IAI institut für Automatisierung und Informatik (GmbH) Wernigerode (Germany).

Paolo Mercorelli has been with the Faculty of Automotive Engineering, Ostfalia University of Applied Sciences, Robert Koch Platz 12, D-38440 Wolfsburg, Germany. p.mercorelli@ostfalia.de

II. DESIGN SPECIFICATIONS AND ACTUATOR DESIGN

The typical valve movement required by engine operation is shown in Fig. 1. The variable stroke needed is between 0 and $8\ \mathrm{mm}$ and is to be realised within a time interval of about $4\ \mathrm{ms}$. Thus, high accelerations up to $4,000\ \mathrm{m/s^2}$ have to be achieved, even in the case of large disturbances due to a strong cylinder pressure acting against the exhaust valve opening. For this reason, high forces coupled with a low moving mass are essential for actuator design.

As the main design goal was to have a high acceleration and low power loss at the same time, we used the following quality function Q as the design criterion to be minimised:

$$Q = \frac{P_v}{a} = \frac{P_v m}{F}, \tag{1}$$

where P_v is the copper loss, a is the possible acceleration, m is the mass (moving part of the actuator and the valve), and F is the actuator force. Different permanent-magnet actuator topologies using NdFeB magnets were considered for the design. In this paper, we present a design study based on the following moving-magnet reluctance DC-actuator, whose basic element is shown in Fig. II.

978-1-61284-799-3/11/$26.00 ©2011 IEEE

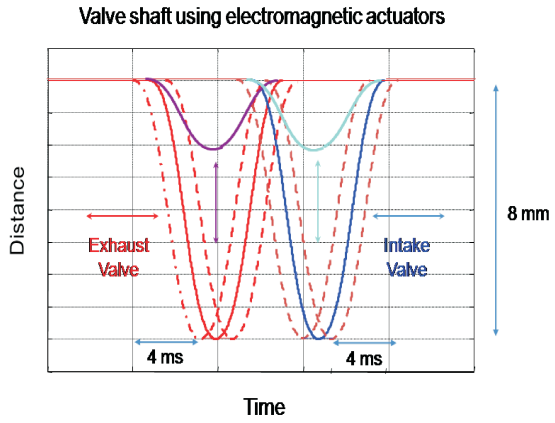

Fig. 1. Opening and closing loop for valve operation

The principle topology of the novel-reluctance linear motor is depicted in Fig. II. The stator of the actuator consists of a laminated iron core divided into two parts with a copper coil embedded in it. The armature sitting between the stator packages is built of thin permanent-magnet plates mechanically connected to each other. We determined during our

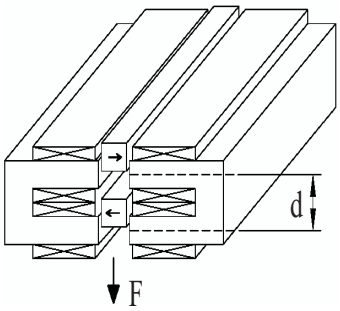

Fig. 2. Basic element of the linear reluctance motor

design process that some optimum can be reached using a four-pole or a six-pole topology. Figure II shows such an actuator arrangement with its calculated force in position and current dependence depicted in Fig. 4. Clearly, combined with the spring, acceleration forces of 600 N or even larger values are possible. Such high forces are needed to open the exhaust valve against the gas pressure coming from the combustion chamber. After having fixed some basic design parameters, the forces were calculated by finite-element calculation, and the quality function Q was evaluated to assess the performance. Subsequently, iterative calculations based on an optimisation strategy were carried out to optimise the design step-by-step, also taking into account the nonlinear saturation and leakage effects. The iteration was also supported by dynamic simulations to determine the overall power loss during a total engine operation cycle at different speeds. At the end of

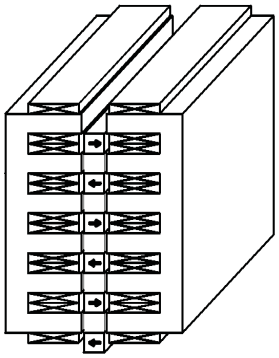

Fig. 3. Actuator with 6 poles (valve position at -4 mm, i.e. in the opened position)

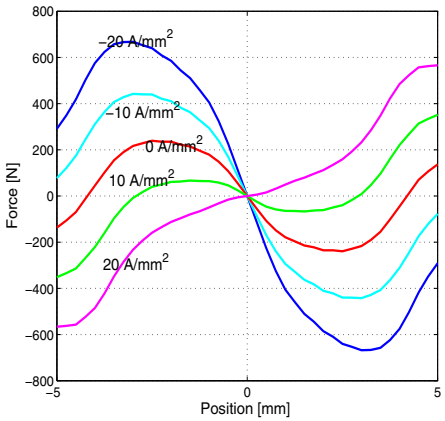

Fig. 4. Reluctance force depending on position and current densities in a 6-pole motor (negative force - moving down)

this process, a novel linear reluctance actuator with excellent dynamic parameters and low power losses was derived. Figure 5 shows the mechanical structure of the actuator connected with the engine valve. In Table 1, some of the most interesting parameters of the developed actuator are given. It is easy to recognise that the specified technical characteristics were fully reached.

III. Description of the Model

The electromagnetic actuator depicted in the left part of Fig. II can be modelled mathematically in the following way:

$$\frac{di_{\text{Coil}}(t)}{dt} = -\frac{R_{\text{Coil}}}{L_{\text{Coil}}} i_{\text{Coil}}(t) + \frac{u_{in}(t) - u_q(t)}{L_{\text{Coil}}}, \tag{2}$$

$$\frac{dy(t)}{dt} = v(t), \tag{3}$$

$$\frac{dv(t)}{dt} = \frac{f(i_{\text{Coil}}(t), y(t))}{m} i_{\text{Coil}}(t) + \frac{-k_d v(t) - k_f y(t) + F_0(t)}{m}, \tag{4}$$

where

$$f(y(t), i_{Coil}(t)) = F_{sin}(y(t)) + F_L(y(t), i_{Coil}(t)) \tag{5}$$

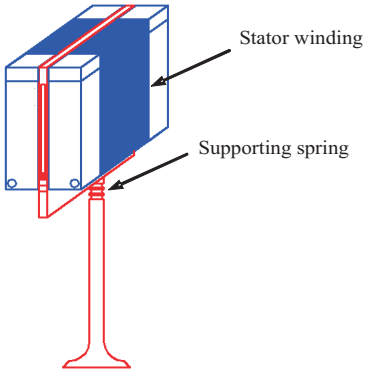

Fig. 5. Mechanical structure with valve coupling

TABLE I
PARAMETERS OF THE ACTUATOR (6 POLES)

Moving mass: (including an 50 g valve)	157 g
maximum opening force (for -20 A/mm^2)	625 N
maximum acceleration loss per acceleration quality function Q Ws^2/m	3981 m/s^2 0.015
Dimensions: W $*$ H $*$ D mm	36 * 61.5 *100
volume:	222 mm^3
magnet mass:	60 g
copper wire: stator iron package:	48 m (ca. 0.4 kg) 490 g

with the following approximation equations

$$F_{\sin}(y(t)) = F_{0,max}\sin(2\pi y(t)/d) \tag{6}$$

$$\text{and} \quad F_L(y(t), i_{Coil}(t)) = k_1\big(y(t) + sign(y(t))k_2\big)i_{Coil}(t). \tag{7}$$

k_1 and k_2 are physical constants. The non-linear electromagnetic force generation can be separated into two parallel blocks, $F_{sin}(y(t))$ and $F_L(y(t), i_{Coil}(t))$, corresponding to the reluctance effect and the Lorentz force, respectively. R_{Coil} and L_{Coil} are the resistance and the inductance, respectively, of the coil windings, $u_{in}(t)$ is the input voltage and $u_q(t)$ is the induced emf. $i_{Coil}(t)$, $y(t)$, $v(t)$ and m are the coil current, position, velocity and mass of the actuator respectively, while $k_d v(t)$, $k_f y(t)$ and $F_0(t)$ represent the viscous friction, the total spring force and the disturbance force acting on the valve, respectively.

IV. A REDUCED-ORDER VELOCITY OBSERVER

As discussed above, the proposed technique avoids a more complex non-linear observer, as proposed in Refs. [8] and [9]. An approximated reduced-order velocity observer is built from equation 2. This technique avoids the need for a complete observer and yields to an particular control strategy. If the electrical part of the system is considered, then

$$\frac{di_{\text{Coil}}(t)}{dt} = -\frac{R_{\text{Coil}}}{L_{\text{Coil}}}i_{\text{Coil}}(t) + \frac{u_{in}(t) - C\phi(y(t))v(t)}{L_{\text{Coil}}}; \tag{8}$$

considering that $C\phi(y(t)) = k_1(y(t) + sign(y(t))k_2$, and that if $y(t) = 0 \rightarrow sign(y(t)) = +1$, then $\forall\ y(t)\ C\phi(y(t)) = k_1(y(t) + sign(y(t))k_2 \neq 0$, it follows that

$$v(t) = -\frac{L_{Coil}\frac{di_{\text{Coil}}(t)}{dt} + R_{\text{Coil}}i_{\text{Coil}}(t) - u_{in}(t)}{C\phi(y(t))}. \tag{9}$$

Consider the following dynamic system

$$\frac{d\hat{v}(t)}{dt} = -\mathcal{K}\hat{v}(t) - \mathcal{K}\frac{L_{Coil}\frac{di_{\text{Coil}}(t)}{dt} + R_{\text{Coil}}i_{\text{Coil}}(t) - u_{in}(t)}{C\phi(y(t))}, \tag{10}$$

where $\mathcal{K}$ is a function to be calculated. If the error on the velocity is defined as the difference between the true and the observed velocity, then:

$$e_v(t) = v(t) - \hat{v}(t) \tag{11}$$

and

$$\frac{de_v(t)}{dt} = \frac{dv(t)}{dt} - \frac{d\hat{v}(t)}{dt}. \tag{12}$$

If the following assumption is given:

$$\|\frac{dv(t)}{dt}\| << \|\frac{d\hat{v}(t)}{dt}\|, \tag{13}$$

then in Eq. (12), the term $\frac{dv(t)}{dt}$ is negligible. Using equation (10), Eq. (12) becomes

$$\frac{de_v(t)}{dt} = \mathcal{K}\hat{v}(t) + \mathcal{K}\frac{L_{Coil}\frac{di_{\text{Coil}}(t)}{dt} + R_{\text{Coil}}i_{\text{Coil}}(t) - u_{in}(t)}{C\phi(y(t))}. \tag{14}$$

Remark 1: Assumption (13) states that the dynamics of the approximating observer should be faster than the dynamics of the physical system. This assumption is typical for the design of observers. □

Because of Eq. (9), (14) can be written as follows:

$$\frac{de_v(t)}{dt} = \mathcal{K}\hat{v}(t) - \mathcal{K}v(t)$$

and considering (11), then

$$\frac{de_v(t)}{dt} + \mathcal{K}e_v(t) = 0 \tag{15}$$

$\mathcal{K}$ can be chosen to make Eq. (15) exponentially stable. To guarantee exponential stability, $\mathcal{K}$ must be

$$\mathcal{K} > 0.$$

To guarantee $\|\frac{dv(t)}{dt}\| << \|\frac{d\hat{v}(t)}{dt}\|$, then $\mathcal{K} >> 0$. The observer defined in (10) suffers from the presence of the derivative of

the measured current. In fact, if measurement noise is present in the measured current, then undesirable spikes are generated by the differentiation. The proposed algorithm needs to cancel the contribution from the measured current derivative. This is possible by correcting the observed velocity with a function of the measured current, using a supplementary variable defined as

$$\eta(t) = \hat{v}(t) + \mathcal{N}(i_{\text{Coil}}), \tag{16}$$

where $\mathcal{N}(i_{\text{Coil}})$ is the function to be designed.

Consider

$$\frac{d\eta(t)}{dt} = \frac{d\hat{v}(t)}{dt} + \frac{d\mathcal{N}(i_{\text{Coil}})}{dt} \tag{17}$$

and let

$$\frac{d\mathcal{N}(i_{\text{Coil}})}{dt} = \frac{d\mathcal{N}(i_{\text{Coil}})}{di_{\text{Coil}}}\frac{di_{\text{Coil}}(t)}{dt} = \mathcal{K}\frac{L_{Coil}}{C\phi(y(t))}\frac{di_{\text{Coil}}(t)}{dt}. \tag{18}$$

The purpose of (18) is to cancel the differential contribution from (10). In fact, (16) and (17) yield, respectively,

$$\hat{v}(t) = \eta(t) - \mathcal{N}(i_{\text{Coil}}) \quad \text{and} \tag{19}$$

$$\frac{d\hat{v}(t)}{dt} = \frac{d\eta(t)}{dt} - \frac{d\mathcal{N}(i_{\text{Coil}})}{dt}. \tag{20}$$

Substituting (18) in (20) results in

$$\frac{d\hat{v}(t)}{dt} = \frac{d\eta(t)}{dt} - \mathcal{K}\frac{L_{Coil}}{C\phi(y(t))}\frac{di_{\text{Coil}}(t)}{dt}. \tag{21}$$

Inserting Eq. (21) into Eq. (10) the following expression is obtained[1]:

$$\frac{d\eta(t)}{dt} - \mathcal{K}\frac{L_{Coil}}{C\phi(y(t))}\frac{di_{\text{Coil}}(t)}{dt} = -\mathcal{K}\hat{v}(t) - \mathcal{K}\frac{L_{Coil}\frac{di_{\text{Coil}}(t)}{dt} + R_{\text{Coil}}i_{\text{Coil}}(t) - u_{in}(t)}{C\phi(y(t))}; \tag{22}$$

then

$$\frac{d\eta(t)}{dt} = -\mathcal{K}\hat{v}(t) - \mathcal{K}\frac{R_{\text{Coil}}i_{\text{Coil}}(t) - u_{in}(t)}{C\phi(y(t))}. \tag{23}$$

Letting $\mathcal{N}(i_{\text{Coil}}(t)) = k_{app}i_{\text{Coil}}(t)$, where with k_{app} a parameter has been indicated, then, from (18) $\Rightarrow \mathcal{K} = \frac{k_{app}}{L_{Coil}}C\phi(y(t))$, Eq. (19) becomes

$$\hat{v}(t) = \eta(t) - k_{app}i_{\text{Coil}}(t). \tag{24}$$

Finally, substituting (24) into (23) results in the following equation

$$\frac{d\eta(t)}{dt} = -\frac{k_{app}}{L_{Coil}}C\phi(y(t))\big(\eta(t) - k_{app}i_{\text{Coil}}(t)\big) + \frac{k_{app}C\phi(y(t))}{L_{Coil}}\Big(u_{in}(t) - R_{\text{Coil}}i_{\text{Coil}}(t)\Big),$$

$$\hat{v}(t) = \eta(t) - k_{app}i_{\text{Coil}}(t). \tag{25}$$

Remark 2: If $y(t) \geq 0$, then $C\phi(y(t)) > 0$, condition $\lim_{t\to\infty} e_v(t) = v(t) - \hat{v}(t) = 0$ is always guaranteed for $k_{app} > 0$. In fact, under condition (13), the system described in (25) satisfies condition (15) by construction. If $y(t) < 0$, then $C\phi(y(t)) < 0$, $\lim_{t\to\infty} e_v(t) = v(t) - \hat{v}(t) = 0$ is always guaranteed for $k_{app} < 0$. □

Remark 3: Condition (13) states apparently a limit on the functionality of the conceived observer. In fact, it seems that condition (13) cannot be satisfied at steady state. In real case, observer (25) never achieves a steady state condition. This is also visible from the simulations at the end of the paper. In these simulations at condition $v(t) = 0$, the observed velocity $\hat{v}(t)$ begins to oscillate with a mean value equal to zero. It is to be noticed that for $v(t) = 0$ the system is not observable and thus it is not to be pretended to have an estimation error equal to zero. Since the entire observer algorithm depends on this assumption, in the section of the simulations this issue is addressed carefully. □

Using the implicit Euler method, the following velocity observer structure is obtained:

$$\eta(k) = \frac{\eta(k-1)}{1 + t_s\frac{k_{app}C\phi(y(k))}{L_{Coil}}} + \frac{t_s\frac{k_{app}^2C\phi(y(k))}{L_{Coil}} - \frac{t_sR_{\text{Coil}}k_{app}C\phi(y(k))}{L_{Coil}}}{1 + t_s\frac{k_{app}C\phi(y(k))}{L_{Coil}}}i_{\text{Coil}}(k) + \frac{t_s\frac{k_{app}C\phi(y(k))}{L_{Coil}}}{1 + t_s\frac{k_{app}C\phi(y(k))}{L_{Coil}}}u_{in}(k),$$

$$\hat{v}(k) = \eta(k) - k_{app}i_{\text{Coil}}(k), \tag{26}$$

where t_s is the sampling period. The velocity observer described in Eq. (26) is utilized as a switching one. If $y(t) < 0$, then $k_{app} < 0$, if $y(t) \geq 0$, then $k_{app} > 0$. In Fig. (6) a conceptual scheme of this observer is shown.

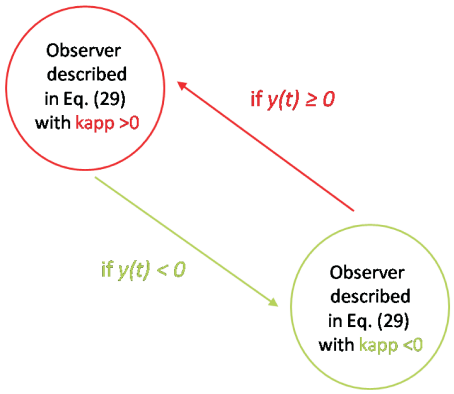

Fig. 6. Conceptual switching observer scheme

V. Actuator Control

Figure 7 shows the control structure applied to the actuator. The actuator consists of three parts from the control point

[1]Expression (10) works under the assumption (13): fast observer dynamics.

of view: an electrical system (motor coil), an electromagnetic system (generation reluctance force) and a mechanical system (mass-spring-damper), with the back emf as an internal voltage feedback for the electrical system. Under normal operating conditions, the electrical subsystem is linear and can be represented by the transfer function

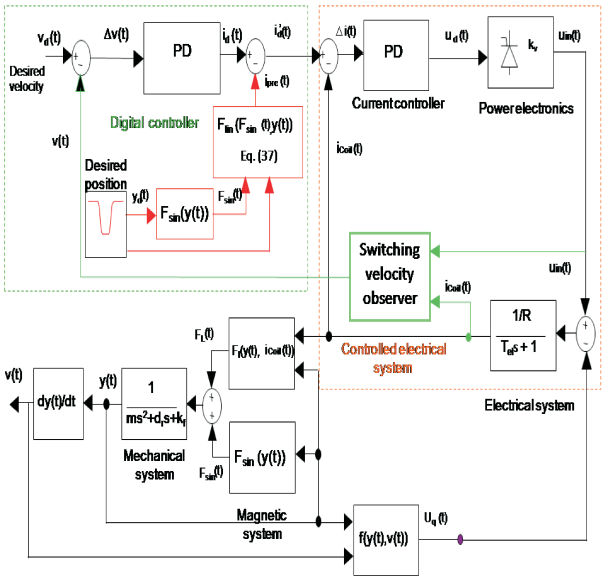

Fig. 7. Control structure

$$G_{el} = \frac{1/R}{Ts+1} \tag{27}$$

where R is the resistance, and T is the time-constant of the coil. The mechanical subsystem is characterized by

$$G_m(s) = \frac{Y(s)}{F(s)} = \frac{1}{ms^2 + ds + k_s}, \tag{28}$$

with the moving mass m, the viscose damping factor d and the spring constant k_s. $Y(s)$ and $F(s)$ are the Laplace transformations of the position $y(t)$ and of the force defined by Eq. (5) respectively. Because the system damping is very weak, it is obviously up to the control to enable a well-damped overall system. The control structure basically consists of two PD controllers organised in a cascade scheme. PD regulators are often utilised in control problems where a high dynamic range is required. The internal loop is devoted to the current control and provides a compensation of the electrical system, which is the fastest time constant of the physical system. Due to the very high dynamic range required by the valve actuation, the current control loop was realised in an analogue technique. The external loop is a PD controller on the velocity. This and the trajectory generation and the position control were implemented on a DSP. For the implemented kind of control strategy is the existence of steady-state error a problem. As shown in Fig. 7, a nonlinear feed-forward block, containing the inverse reluctance characteristics, was used to compensate for the nonlinear effects of the actuator and to ensure the stationary accuracy. In fact, having compensated for the nonlinearities, the overall system behaviour can be approximated by a linear third-order system. In particular, the nonlinear compensation is performed while generating the desired current from the inversion of the linear part of the motor characteristic, as described in the following:

$$i_{pre}(t) = \frac{F_L(t)}{k_1(y_d(t) + sign(y_d(t))k_2)}. \tag{29}$$

The inversion of the force-position characteristic of the motor leads to the total actuator force, from which its sinusoidal non-linear part is then subtracted:

$$F_L(t) = ky_d(t) + d\dot{y}_d(t) + m\ddot{y}_d(t) - F_{0,max}\sin(2\pi y_d(t)/d) \tag{30}$$

Finally the following equation is obtained:

$$i_{pre}(t) = \frac{ky_d(t) + d\dot{y}_d(t) + m\ddot{y}_d(t)}{k_1(y_d(t) + sign(y_d(t))k_2)} \\ \frac{-F_{0,max}\sin(2\pi y_d(t)/d)}{k_1(y_d(t) + sign(y_d(t))k_2)}. \tag{31}$$

Based on the desired position signal coming out of the trajectory generator and the measured valve position, a PD-type position controller (lead compensator) is applied. Contrary to the conventional position control in drive systems, where PI-type controllers are mostly used, in this special case we need to increase substantially the exiting phase margin to achieve the desired system damping.

VI. Simulations

Here, some typical simulation results using the control structure described above are presented in Fig. 7. For the opening phase, a strong but rapidly decreasing gas pressure is assumed to be present and is simulated as an unknown disturbance. Even though the presented control strategy does not consider this disturbance condition, the system shows excellent control behaviour. In the simulation, a realistic white noise in the measurement of the current is considered. The typical control behaviour is demonstrated in Fig. 10, where a full-range operation cycle at an engine speed of 3000 rpm (rounds per minute) is shown. Here, high tracking accuracy is demonstrated despite the noise which was introduced for the simulation. The input current and input voltage (see Figs. 9 and 8) present noise due to the derivative effect of the controller. Theoretically and in computer simulations, control precision can be further improved by increasing the gain of the controllers. However, measurement noises can cause serious oscillations, which may lead to local stability problems in practical situations. The entire observer algorithm depends on assumption (13), which states apparently a limit on the functionality of the conceived observer . In fact, it seems that condition (13) cannot be satisfied at steady state. In real case, observer (25) never achieves a steady state condition. This is also visible from Fig. 10. In these simulations it is visible at the points in which the position remains constant ($v(t) = 0$),

the observed velocity $\hat{v}(t)$ begins to oscillate with a mean value equal to zero. It is worthwhile to notice again, that for $v(t) = 0$ the system is not observable ant thus it is not to be pretended to have an estimation error equal to zero.

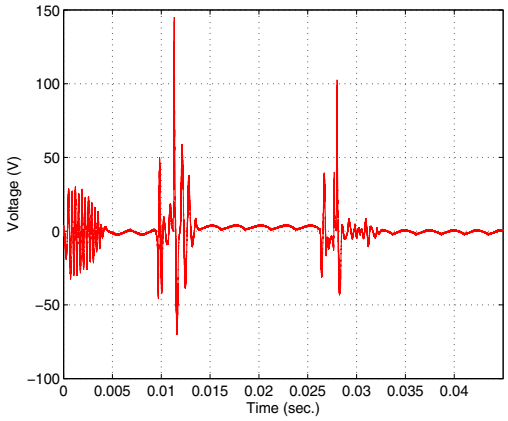

Fig. 8. Closed loop input voltage

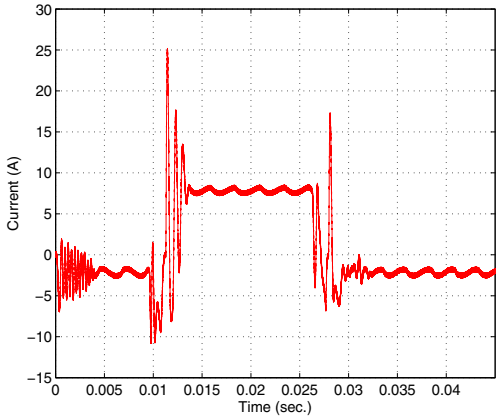

Fig. 9. Closed loop coil current

VII. Conclusions and Future Works

The design of a novel linear reluctance motor using permanent-magnet technology is presented to be used in automotive applications. The developed actuator is specifically intended to be used as an electromagnetic engine valve drive. Besides a design analysis, the structure and properties of the applied control strategy are also discussed. Dynamic simulation results of a sensorless control strategy are presented and show good performance. In particular, based on a nonlinear model, an observer is presented that achieves sensorless control. This paper presents feasible real-time approximated velocity estimator based on measurements of input current and input voltage. A control strategy is presented and discussed as well. Computer simulations of the sensorless control structure are presented, in which are visible in the closed-loop control.

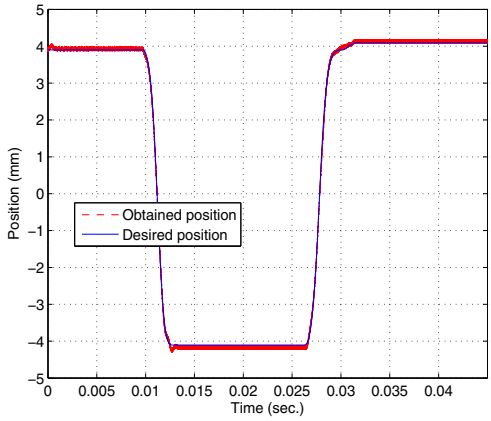

Fig. 10. Controlled position

A. Future Works

Future works could be oriented towards analysis of the stability of the whole closed-loop structure (plant-observer-controller). This analysis could provide useful indications in the determination of the parameters of the controllers. Moreover, a possible parametrization of this velocity observer could be used and optimised using a technique similar to that presented in Ref. [10]. Future work should also include investigations of a reduced-order observer in order to avoid the measurement of the position. The idea is to measure the input current and the input voltage to estimate position and velocity. Moreover, experimental measurements under real engine conditions are to be done.

References

[1] C. Tai and T. Tsao. Control of an electromechanical actuator for camless engines. In *Proceedings of the American control conference*, 2003.

[2] Peterson K.S. *Control Methodologies for Fast & Low Impact Electromagnetic Actuators for Engine Valves*. PhD Thesis, University of Michigan, 2005.

[3] S. Braune, S. Liu, and P. Mercorelli. Design and control of an electromagnetic valve actuator. In *Proceedings of 2006 IEEE International Conference on Control Applications*, pages 1657–1662, Munich (Germany), 4th-6th October 2006.

[4] R. Wu and G.R. Slemon. A permanent magnet motor drive without a shaft sensor. *IEEE Transactions on Industrial Applications*, 27:1005–1011, 1991.

[5] G Zhu, A. Kaddouri, L.A. Dessaint, and O. Akhrif. A nonlinear state observer for the sensorless control of a permanent-magnet ac machine. *IEEE Transactions on Industrial Electronics*, 48(6):1098–1108, 2001.

[6] R. Rajamani. Observers for lipschitz nonlinear systems. *IEEE Transactions on Automatic Control*, 43(3):397–401, 1998.

[7] F.E. Thau. Observing the state of nonlinear dynamic systems. *Int. J. of Control*, 17(3):471–479, 1973.

[8] O.H. Dagci, Y. Pan, and U. Ozguner. Sliding mode control of electronic throttle valve. In *Proceedings of the 2002 American Control Conference*, volume 3, pages 1996– 2001, 2002.

[9] A. Beghi, L. Nardo, and M. Stevanato. Observer-based discrete-time sliding mode throttle control for drive-by-wire operation of a racing motorcycle engine. *Control Systems Technology, IEEE Transactions*, 14(4):767– 775, July 2006.

[10] P. Mercorelli. Robust feedback linearization using an adaptive pd regulator for a sensorless control of a throttle valve. *Mechatronics a journal of IFAC. Elsevier publishing*, 19(8):1334–1345, 2009.